Enhanced magneto-optical Kerr effects in Py/Ag/Bi trilayers

Patricia Riego[1] [2], Satoshi Tomita[3]‡, Kaoru Murakami[3], Toshiyuki Kodama[3], Nobuyoshi Hosoito[3], Hisao Yanagi[3] and Andreas Berger[1]

[1] CIC nanoGUNE, E-20018 Donostia-San Sebastian, Spain

[2] Departamento de la Física de la Materia Condensada, Universidad del País Vasco, UPV/EHU, E-48080 Bilbao, Spain

[3] Graduate School of Materials Science, Nara Institute of Science and Technology, Nara 630-0192, Japan

E-mail: tomita@ms.naist.jp

January 2017

Abstract. We study the magneto-optical (MO) response of permalloy/silver/bismuth (Py/Ag/Bi) trilayer samples in reference to a control Py film by means of spectroscopic generalized MO ellipsometry. The trilayer structures show enhanced MO Kerr amplitude values compared to optical multilayer calculations based upon the Py film reference measurements, especially in the near-infrared region. This indicates that the optical interference conditions accounted for in the model are not sufficient to explain the influence of the Ag/Bi bilayer in the structure. Instead, the local optical and MO properties of the Py layer itself must be modified by the presence of the Ag/Bi bilayer, which could be caused by enhanced effective spin-orbit coupling.

Keywords:magnetic multilayer, spectroscopic generalized magneto-optical ellipsometry, magneto-optical Kerr effect, spin-orbit coupling

Submitted to: *J. Phys. D: Appl. Phys.*

‡ visiting researcher at CIC nanoGUNE, E-20018 Donostia-San Sebastian, Spain

Spin-orbit coupling (SOC) is a key phenomenon in modern magnetism and spintronics. Much attention has been paid recently to the Rashba-type SOC [1] at interfaces [2, 3] or in semiconductor quantum wells [4, 5, 6, 7, 8]. Large values of the Rashba coefficient have been found at interfaces between heavy elements with strong SOC, for example, bismuth (Bi) and antimony (Sb), and non-magnetic metals, for example, silver (Ag) [9]. In transport measurements, the Ag/Bi interface with a ferromagnetic permalloy (Py) layer gives rise to a very large spin-charge conversion [10, 11], due to the Rashba-type SOC at the interface [12], which is one order of magnitude larger than the conversion parameter in the Ag/Sb interface with a Py layer [13].

From the microscopic point of view, SOC is related to magneto-optical (MO) properties [14, 15, 16, 17] as well as to electron transport. Indeed, enhanced infrared MO response by bulk Rashba spin splitting was reported for the nonmagnetic semiconductor BiTeI [18]. However, enhanced MO responses in the ferromagnetic Py in proximity to a Ag/Bi Rashba interface have not yet been explored. In this Letter, we study Py/Ag/Bi trilayers by means of generalized MO ellipsometry (GME) [19, 20, 21, 22, 23, 24, 25]. GME's main advantage is the ability to study complex MO parameters with unprecedented precision, because it allows one to determine optical and MO properties simultaneously. In addition, the dispersion of the parameters can be obtained through spectroscopic GME (S-GME) measurements [26, 27]. Our experiments reveal that the presence of the Ag/Bi bilayer enhances the MO response of adjacent Py layers, particularly in the near-infrared region.

Figure 1 illustrates sample structures employed in this study. Py, Bi, and Ag layers were deposited onto silicon substrates at room temperature using magnetron sputtering with an argon gas pressure of 4.2×10^{-3} Torr. The Py, Bi, and Ag deposition rates were 0.10, 0.15, and 0.25 nm/s, respectively. In the trilayer sample labeled PSB1 as shown in figure 1(a), a Bi layer having 10 nm in thickness was deposited on the Si substrate first, after which a Ag layer of 5 nm and a Py layer of 30 nm thickness were sequentially deposited. The other trilayer sample, which is labeled PSB2, has an inverted structure as shown in figure 1(b), meaning that a 5 nm thick Ag layer was sputtered onto the initially deposited Py layer, which was furthermore covered by a Bi layer of 10 nm thickness. The control sample has only a Py layer with 30 nm thickness [figure 1(c)]. All samples were coated by a 2 nm thick tantalum (Ta) layer to avoid oxidization of the functional layers.

The determination of magneto-optical and optical properties was achieved by means of S-GME. Previous implementations of S-GME [26, 27] utilized a discharge lamp and a grating spectrometer for investigating the wavelength dependence. In turn, our approach here is to use a wavelength tunable laser and to perform measurements at different wavelengths in the visible and near-infrared regions.

The experimental setup is illustrated schematically in figure 2. A Fianium wavelength-tunable laser in combination with a computer-controlled acousto-optically tunable filter (AOTF) was used for the generation of a monochromatic light beam in the

wavelength (λ) range between 450 and 850 nm. In order to obtain the desired mechanical stability and facilitate the alignment of the setup, an optical fiber was utilized to direct the light exiting the AOTF, onto the sample with an incidence angle of 45°. After the fiber aperture, the beam passed through a rotatable broadband linear polarizer P_1, was then reflected by the sample surface, and passed through the second rotatable broadband polarizer P_2 in the exact same way as in a standard GME experiment [19, 20, 23, 25]. Given the usage of the optical fiber, additional broadband focusing lenses were inserted into the light path before P_1 and after P_2, as shown in figure 2, in order to focus the beam spot on the sample surface and finally onto the detector. The light intensity after P_2 was detected by a low-background Si photodiode with a responsivity spectrum that matches appropriately the spectral range of the laser. Given that λ of the laser was scanned during the S-GME operation, the detector was equipped with a tube-like geometrical filter for isolation from ambient light, rather than the monochromatic filter used in conventional GME [23, 25].

The samples were placed between the poles of an electromagnet. The electromagnet generated a magnetic field of up to ± 1.1 kOe, which was more than sufficient to saturate our samples. The field was applied along the x-axis, i.e., it was contained in the plane-of-incidence and in the plane of the sample, giving rise to the longitudinal MO Kerr effect (MOKE) configuration. The operation of our S-GME, which is automatized and computer-controlled, consists of performing sequentially standard GME measurements for different λ, i.e., of measuring for each λ value the normalized change in light intensity $\delta I/I$ upon magnetization reversal for different combinations of P_1 and P_2 orientations. With the subsequent analysis described in Refs. [19, 20, 23, 25], these measurements allow us to determine the complete reflection matrix of the sample at different λ. Specifically, they permit us to retrieve the spectral dependence of the Kerr rotation θ_K and Kerr ellipticity ϵ_K at the magnetic saturation state of the sample, which are the key quantities that we utilize in this study.

Our three samples have been characterized in detail using this S-GME setup. As an example of the collected data, the left column of figure 3 highlights experimental $\delta I/I$ maps as a function of θ_1 and θ_2 for the PSB1 sample in saturation at different λ. Figures 3(a), 3(b), and 3(c) correspond to measured maps at λ = 450, 600, and 800 nm, respectively. Hereby, the red color corresponds to positive $\delta I/I$ while the blue color represents negative $\delta I/I$. The measured patterns exhibit two lobes of opposite sign that meet at the crossing point of the polarizers at $\theta_1 = 90°$ and $\theta_2 = 0°$, which is a signature of the longitudinal MOKE signal. As is evident from figures 3(a)-3(c), $\delta I/I$ depends very much on the λ utilized to perform the measurements. On the one hand, its magnitude is different for different λ, as one can see in the scale bars next to figures 3(d)-3(f). The shape of the lobe-like features as a function of θ_1 and θ_2 also changes with λ.

A multiparameter least-squares fitting procedure [19] of the data in figures 3(a)-3(c) enables us to extract the reflection matrix, which for an in-plane magnetized sample as

ours reads

$$R = \begin{pmatrix} r_s & \alpha \\ -\alpha & r_p + \beta \end{pmatrix}. \quad (1)$$

From the reflection matrix elements in equation (1), we evaluate the Kerr rotation $\theta_K = \mathrm{Re}(\alpha/r_p)$ and ellipticity $\epsilon_K = \mathrm{Im}(\alpha/r_p)$ for incoming p-polarized light. The sign convention for θ_K and ϵ_K is the same as in reference [28]. The fitted $\delta I/I$ maps are shown in figures 3(d)-3(f), in a side-by-side comparison with the experimental data. The quality of the fittings is excellent, and the R^2 goodness of the fits is very close to 1 as shown in the inset of figures 3(d)-3(f).

With the $\theta_K(\lambda)$ and $\epsilon_K(\lambda)$ values obtained from the fits of the $\delta I/I$ maps, we have evaluated the Kerr amplitude $|\Theta_K(\lambda)| = \sqrt{[\theta_K(\lambda)]^2 + [\epsilon_K(\lambda)]^2}$. $|\Theta_K(\lambda)|$ spectra for our three samples are depicted in figure 4(a) for the incidence angle of 45° that we utilized. Overall, the three samples show a decrease in $|\Theta_K(\lambda)|$ at a longer λ. Experimental results in figure 4(a) demonstrate that the PSB2 sample (blue circles) has a smaller $|\Theta_K(\lambda)|$ than the control sample (black triangles) over all the explored spectral range. This seems to be consistent with the fact that the ferromagnetic Py layer is now buried below 5 nm of Ag and 10 nm of Bi, which are not magneto-optically active themselves, and thus the overall MO signal of the sample is reduced.

The PSB1 sample (red squares), however, in which the Py layer has an Ag/Bi underlayer, shows an enhanced $|\Theta_K(\lambda)|$ at every λ with respect to the reference sample. In order to make this enhancement clearer, we have normalized $|\Theta_K(\lambda)|$ of the PSB1 and PSB2 samples to the one of the control sample. The experimentally observed "enhancement factor" $|\Theta_K(\lambda)|/|\Theta_K(\lambda)|(Control)$ is shown in figure 4(b) as a function of λ in red squares for PSB1 and blue circles for PSB2. For PSB1, the enhancement factor for $|\Theta_K(\lambda)|$ is 1.2 at $\lambda = 450$ nm and increases up to 1.4 at a longer λ in the near-infrared region. On the other hand, for PSB2, the enhancement factor is smaller than one for all values of λ, starting at approximately 0.5 at $\lambda = 450$ nm and increasing modestly to 0.6 for a longer λ.

In principle, the enhanced $|\Theta_K(\lambda)|$ of the PSB1 sample could be caused by a modification of the material properties of the magneto-optically active material, i.e., Py. However, that is not the only possible explanation due to the fact that while $|\Theta_K(\lambda)|$ arises from the Py layer, its value is also affected by the overall sample structure. In general, reflection properties of a sample including MO effects depend on the different materials in a sample and their stacking order by means of optical interference conditions at material interfaces, which can enhance or weaken $|\Theta_K(\lambda)|$. In order to check whether the mere material stacking can explain the observed changes in $|\Theta_K(\lambda)|$, we have performed calculations based on a transfer matrix method [29, 30] to mimic the reflection experiments carried out for our samples. By solving Maxwell's equations with the appropriate boundary conditions at the material interfaces, this method allows for the determination of the optical and MO properties of the structures under study. The model incorporates the exact treatment of classical electromagnetic

light penetration in a multilayer stack, thus intrinsically accounting for the effects of the penetration depth of light.

In such a way, we have calculated $|\Theta_K(\lambda)|$ of Si/Py, Si/Py/Ag/Bi, and Si/Bi/Ag/Py multilayers assuming the nominal structure of our samples and our experimental conditions, i.e., layer and substrate thicknesses, incident angle, λ, and magnetization orientation. In the modeling, literature values of Si, Ag and Bi optical parameters [31, 32] were utilized. We used the optical and MO parameters of Py obtained from a 60-nm-thick Py film deposited under the same conditions as the Py in the specific samples studied here, assuming that this thicker Py film represents a bulk-type system. These calculations do not correspond to a fit of the experimental data. Instead, the goal of the modelling is to show what the expected MO signal of our samples would be, if the classical exact solution of the electromagnetic wave equation in the presence of a multilayered material were describing completely the system.

The model calculations of the $|\Theta_K(\lambda)|/|\Theta_K(\lambda)|(Control)$ ratios are displayed with solid lines in gure 4(b) for the Si/Bi/Ag/Py (red solid line) and Si/Py/Ag/Bi (blue solid line) structures. These calculations based on the classical solution of Maxwell's equation in multilayered structures reproduce qualitatively the fact that $|\Theta_K(\lambda)|$ in the trilayer with Py on top of an Ag/Bi bilayer is enhanced with respect to the control sample with only Py, while the inverted trilayer with Py under the Ag/Bi bilayer has a reduced $|\Theta_K(\lambda)|$ with respect to the reference. However, a quantitative comparison shows that the model underestimates the enhancement factors if compared to the experiment, and does so for both trilayer structures. The deviations in between the model and the experiment clearly indicate that a key aspect of the physical behavior is missing in the model, which only accounts for the optical interference due to the material stacking and does not take into account possible modifications of optical properties of the material due to interfacial effects.

To check the reliability of our model prediction and our conclusions that we observe an anomalously enhanced experimental effect, we have performed several tests by allowing for changes in the modeled structures. First, we have studied whether a hypothetical difference in thickness of the Py layers in PSB1 and PSB2 as compared to the Py layer control sample could affect our conclusions. For example, even if the Py thickness is nominally the same in all the samples, the different deposition sequences could lead to a different layer intermixing for the different interfaces, and thus to an actual change of the effective thickness of the Py layer. While it was reported that the metallic Ta cap layer results in a loss of moment of the Py layer equivalent to a dead layer of thickness about 1 nm[33], this is not significant in the present PSB1 sample with the 30 nm-thick Py layer. Given that the experimental data show larger enhancements than the model for the PSB1 and PSB2 samples, the thickness of the ferromagnetic layer should be thicker in PSB1 and PSB2 than in the control sample, if this were the reason for the experiment to model calculation discrepancy. As a worst case scenario, we have considered a rather massive thickness variation in the Py layers, specifically an only 20 nm-thick Py layer in the control structure, while keeping the 30 nm-thick Py in

the other two structures.

The corresponding recalculated spectra are shown as dashed lines in figure 4(b): the red one corresponding to the Si/Bi/Ag/Py structure, and the blue one to the inverted layer sequence. We observe that the calculated enhancement factors increase for both structures assuming this 10 nm variation in the Py thickness. However, the enhancement values are still below the experimentally observed ones, especially in the near-infrared region, i.e., $\lambda \sim 700$ to 800 nm, where the model gives rise to an enhancement of at most 1.2 for the Si/Bi/Ag/Py sample, while the experiment shows an enhancement of 1.4. A variation in the Py thickness is thus not sufficient to explain enhanced MO properties, and we therefore rule out that layer thickness variations are the source of the observed enhancement.

Additionally, we have studied the effect of deviations from the literature values in the optical constants of Bi or Ag [31, 32]. Specifically, we have found that a simultaneous variation in the refractive index of Bi and Ag of up to 15%, which is a value above typical sample-to-sample variations, cannot explain the observed experimental enhancement either. We have also verified that the inclusion of a 2-nm-thick Ta overcoat does not alter in any significant manner the calculated enhancement ratios shown in gure 4(b).

We therefore conclude that the observed $|\Theta_K(\lambda)|$ enhancement we find for our trilayer structures cannot be explained by optical interference effects. Instead, the large enhancement should be caused by a modication of the optical and/or MO properties of the individual materials that compose the sample. Several works have shown that the deposition of nonmagnetic metal overlayers can modify the magnitude of the Kerr effect or the magneto-crystalline anisotropy in ferromagnetic materials [34, 35, 36, 37, 38, 39]. These two quantities are intimately related to the SOC [14, 40, 41, 15, 16, 17]. In our case, the significant enhancement observed in $|\Theta_K|$ could be ascribed to SOC that arises from the Ag/Bi interface. Last but not least, we should point out that due to the different stacking of the layers in our samples, the growth details of the Py layer could be altered in between the different samples, which might also modify its MO properties to a certain degree. However, a growth induced alternation alone seems to be unlikely to explain our observations, because we observe anomalously enhanced $|\Theta_K(\lambda)|/|\Theta_K(\lambda)|(Control)$ values for both trilayer structures, which have completely different growth sequences. More detailed studies of interface quality using cross-sectional electron microscopic observations are beyond the scope of this article and a further issue.

In conclusion, we observe an enhancement in the MO activity of Py layers with an adjacent Ag/Bi-interface layer. S-GME measurements between $\lambda = 450$ nm and 850 nm demonstrate that the Kerr amplitude $|\Theta_K(\lambda)|$ of the trilayer sample consisting of the Py layer with the Ag/Bi bilayers underneath is larger than that of a control Py layer at every λ with an enhancement factor in the normalized $|\Theta_K(\lambda)|$ of 1.2 at $\lambda = 450$ nm, which increases up to 1.4 for $\lambda = 800$ nm. Calculated $|\Theta_K(\lambda)|$ spectra based on optical models indicate that this enhancement, particularly in the near-infrared region, cannot be quantitatively explained by optical interference in the trilayers and sample to sample

structure variations. On the other hand, while $|\Theta_K(\lambda)|$ of the inverted trilayer structure is smaller than that of the control Py layer, the measured signal is still larger than what one would expect from optical model calculations, which also indicates an MO signal enhancement for the Py due to presence of an adjacent Ag/Bi-interface layer. Thus, we find in our experiments a general MO signal enhancement for trilayer structures, which can be consistently explained by means of enhanced SOC effects in these non-magnetic interface layers altering the MO response of adjacent Py films.

Acknowledgments

This work was supported by JSPS KAKENHI (No. 26287065, No. 16K04881). Work at CIC nanoGUNE was supported by the Basque Government under Project No. PI2015-1-19 and the Spanish Ministry of Economy and Competitiveness under the Project No. FIS2015-64519-R (MINECO/FEDER). P.R. acknowledges Obra Social "la Caixa" for her Ph.D. fellowship. T.K. acknowledges Grant-in-Aid for JSPS Research Fellow.

References

[1] Bychkov Y A and Rashba E I 1984 *JETP Lett.* **39** 7881
[2] Dedkov Y S, Fonin M, Rüdiger U and Laubschat C 2008 *Phys. Rev. Lett.* **100** 107602
[3] Caviglia A D, Gabay M, Gariglio S, Reyren N, Cancellieri C and Triscone J M 2010 *Phys. Rev. Lett.* **104** 126803
[4] Schultz M, Heinrichs F, Merkt U, Colind T, Skaulid T and Løvold S 1996 *Semicond. Sci. Technol.* **11** 1168
[5] Ganichev S D, Bel'kov V V, Golub L E, Ivchenko E L, Schneider P, Giglberger S, Eroms J, De Boeck J, Borghs G, Wegscheider W, Weiss D and Prettl W 2004 *Phys. Rev. Lett.* **92** 256601
[6] Giglberger S, Golub L E, Bel'kov V V, Danilov S N, Schuh D, Gerl G, Rohlfing F, Stahl J, Wegscheider W, Weiss D, Prettl W and Ganichev S D 2007 *Phys. Rev.* B **75** 035327
[7] Li J, Chang K, Hai G Q and Chan K S 2008 *Appl. Phys. Lett.* **92** 152107
[8] Lee T Y, Chang J, Hickey M C, Koo H C, Kim H J, Han S H and Moodera J S 2011 *Appl. Phys. Lett.* **98** 202504
[9] Ast C R, Henk J, Ernst A, Moreschini L, Falub M C, Pacilé D, Bruno P, Kern K and Grioni M 2007 *Phys. Rev. Lett.* **98** 186807
[10] Rojas Sánchez J C, Vila L, Desfonds G, Gambarelli S, Attané J P, De Teresa J M, Magén C and Fert A 2013 *Nature Commn.* **4** 2944
[11] Nomura A, Tashiro T, Nakayama H and Ando K 2015 *Appl. Phys. Lett.* **106** 212403
[12] Edelstein V M 1990 *Solid State Commun.* **73** 233
[13] Zhang W, Jungfleisch M. B, Jiang W, Pearson J. E and Hoffmann A 2015 *J. Appl. Phys.* **117** 17C727
[14] Argyres P N 1955 *Phys. Rev.* **97** 334
[15] Suzuki Y, Katayama T, Yoshida S, Tanaka K and Sato K 1992 *Phys. Rev. Lett.* **68** 3355
[16] Shinagawa K 1999 *Magneto-Optics* (Berlin: Springer)
[17] Kato Y K, Myers R C, Gossard A C and Awschalom D D 2004 *Science* **306** 1910
[18] Demkó L, Schober G A H, Kocsis V, Bahramy M S, Murakawa H, Lee J S, Kézsmárki I, Arita R, Nagaosa N and Tokura Y 2012 *Phys. Rev. Lett.* **109** 167401
[19] Berger A and Pufall M R 1997 *Appl. Phys. Lett.* **71** 965
[20] Berger A and Pufall M R 1999 *J. Appl. Phys.* **85** 4583

[21] Schmidt D, Hofmann T, Herzinger C M, Schubert E and Schubert M 2010 *Appl. Phys. Lett.* **96** 091906
[22] Mok K, Du N and Schmidt H 2011 *Rev. Sci. Instrum.* **82** 033112
[23] Arregi J A, Gonzlez-Díaz J B, Bergaretxe E, Idigoras O, Unsal T and Berger A 2012 *J. Appl. Phys.* **111** 103912
[24] Briley C, Schmidt D, Hofmann T, Schubert E and Schubert M 2015 *Appl. Phys. Lett.* **106** 133104
[25] Riego P, Vélez S, Gomez-Perez J M, Arregi J A, Hueso L E, Casanova F and Berger A 2016 *Appl. Phys. Lett.* **109** 172402
[26] Neuber G, Rauer R, Kunze J, Korn T, Pels C, Meier G, Merkt U, Bäckstörm J and Rübhausen M 2003 *Appl. Phys. Lett.* **83** 4509
[27] Mok K, Kovács G J, McCord J, Li L, Helm M and Schmidt H 2011 *Phys. Rev.* B **84** 094413
[28] Arregi J A, Riego P and Berger A 2017 *J. Phys. D: Appl. Phys.* **50** 03LT01
[29] McGahan W A, Chen L Y, Shan Z S, Sellmyer D J and Woollam J A 1989 *Appl. Phys. Lett.* **55** 2479
[30] Schubert M 1996 *Phys. Rev.* B **53** 4265
[31] Vuye G, Fisson S, Nguyen Van V, Wang Y, Rivory J and Abelès F 1993 *Thin Solid Films* **233** 166
[32] Hagemann H J, Gudat W and Kunz C 1975 *J. Opt. Soc. Am.* **65** 742
[33] Kowalewski M, Butler W. H, Moghadam N, Stocks G. M, Schulthess T. C, Song K. J, Thompson J. R, Arrott A. S, Zhu T, Drewes J, Katti R. R, McClure M. T and Escorcia O 2002 *J. Appl. Phys.* **87** 5732
[34] Beauvillain P, Bounouh A, Chappert C, Mégy R, OuldMahfoud S, Renard J P, Veillet P, Weller D and Corno J 1994 *J. Appl. Phys.* **76** 6078
[35] Buckley M E, Schumann F O and Bland J A C 1995 *Phys. Rev.* B **52** 6596
[36] Hicken R J, Gray S J, Ercole A, Daboo C, Freeland D J, Gu E, Ahmad E and Bland J A C 1997 *Phys. Rev.* B **55** 5898
[37] Bounouh A, Train C, Beauvillain P, Bruno P, Chappert C, Mégy R and Veillet P 1997 *J. Magn. Magn. Mater.* **165** 484
[38] Duden T and Bauer E 1999 *Phys. Rev.* B **59** 468
[39] Kisielewski M, Maziewski A, Tekielak M, Wawro A and Baczewski L T 2002 *Phys. Rev. Lett.* **89** 087203
[40] Misemer D K 1988 *J. Magn. Magn. Mater.* **72** 267
[41] Bertotti G 1998 *Hysteresis in Magnetism, for Physicists, Materials Scientists, and Engineers* (San Diego: Academic Press)

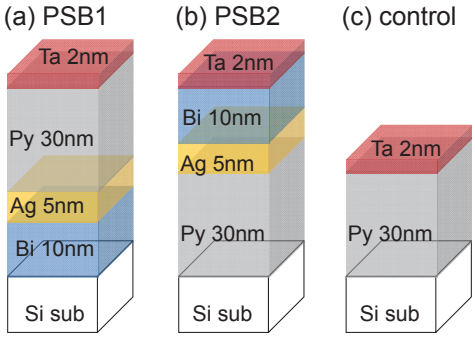

Figure 1. Structures of (a) PSB1 and (b) PSB2 Py/Ag/Bi trilayer samples. The control sample (c) only consists of a Py layer on Si substrate. All samples were coated by a Ta layer.

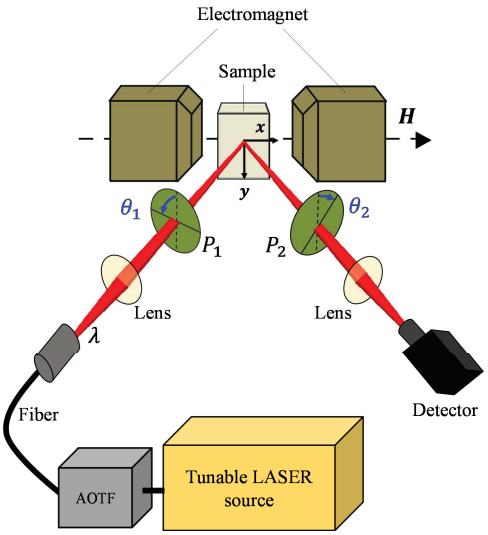

Figure 2. Schematic of our S-GME setup. AOTF: computer-controlled acousto-optically tunable filter, P_1 and P_2: broadband rotatable linear polarizers for incident and reflected light, which are rotated by an angle θ_1 and θ_2, respectively.

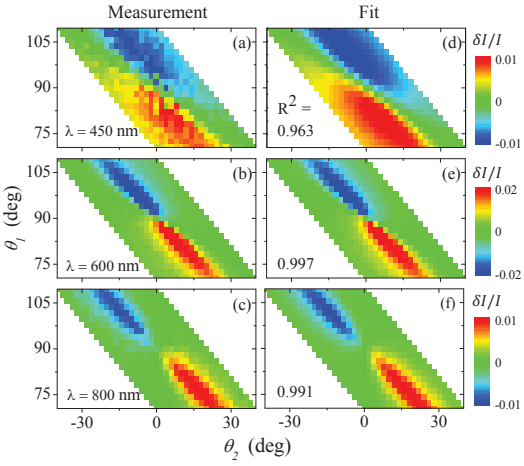

Figure 3. Experimentally measured [(a)-(c)] S-GME maps for PSB1 sample showing $\delta I/I$ as a function of P_1 and P_2 orientations at several wavelength. [(d)-(f)] show the corresponding least-squares fits to the relevant GME-equations [19]. (a) and (d) correspond to $\lambda = 450$ nm, (b) and (e) correspond to $\lambda = 600$ nm, and (c) and (f) correspond to $\lambda = 800$ nm. For each wavelength, the color scale of $\delta I/I$ is indicated on the right-hand side.

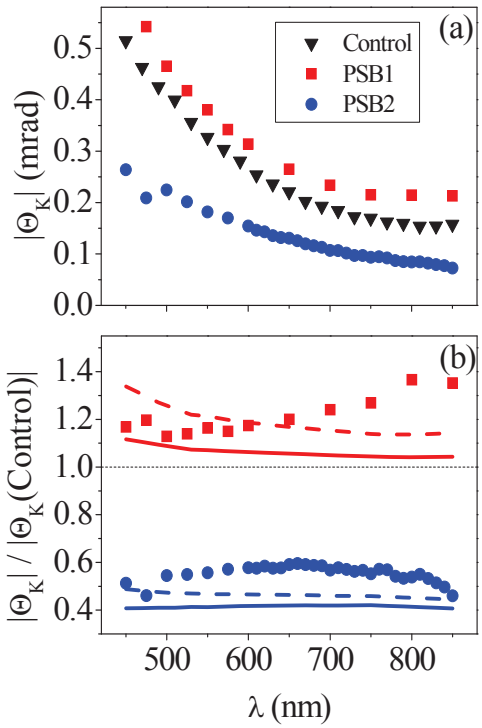

Figure 4. (a) Kerr amplitude $|\Theta_K(\lambda)|$ of PSB1 (red squares), PSB2 (blue circles), and control samples (black triangles). (b) $|\Theta_K(\lambda)|$ of the PSB1 and PSB2 samples normalized to the control sample's $|\Theta_K(\lambda)|$. Experimental values are represented in symbols: red squares and blue circles for PSB1 and PSB2, respectively. The curves show the calculated data from the optical models, in red for PSB1 and in blue for PSB2. The solid lines correspond to the solution of the model with the nominal thickness of the layers, while the dashed curves correspond to the solution of the model considering a control sample with a Py layer that is 33% thinner than the Py layer in the trilayer structures. The lack of agreement between the model and the experimental data indicates that the classical electromagnetic wave equation solution of a multilayered structure is not sufficient to explain the underlying physical behavior of the system.